

Density profiles and collective excitations of a trapped two component Fermi vapour

M. Amoruso¹, I. Meccoli², A. Minguzzi¹ and M. P. Tosi^{1,3*}

¹ *Istituto Nazionale di Fisica della Materia and Classe di Scienze,
Scuola Normale Superiore, Piazza dei Cavalieri 7, 56126 Pisa, Italy*

² *Istituto Nazionale di Fisica della Materia and Dipartimento di Fisica,
Università di Parma, Parco Area delle Scienze 7a, 43100 Parma, Italy*

³ *Abdus Salam International Centre for Theoretical Physics,
Strada Costiera 11, 34014 Trieste, Italy*

Abstract

We discuss the ground state and the small-amplitude excitations of a degenerate vapour of fermionic atoms placed in two hyperfine states inside a spherical harmonic trap. An equations-of-motion approach is set up to discuss the hydrodynamic dissipation processes from the interactions between the two components of the fluid beyond mean-field theory and to emphasize analogies with spin dynamics and spin diffusion in a homogeneous Fermi liquid. The conditions for the establishment of a collisional regime via scattering against cold-atom impurities are analyzed. The equilibrium density profiles are then calculated for a two-component vapour of ⁴⁰K atoms: they are little modified by the interactions for presently relevant values of the system parameters, but spatial separation of the two components will spontaneously arise as the number of atoms in the trap is increased. The eigenmodes of collective oscillation in both the total particle number density and the concentration density are evaluated analytically in the special case of a symmetric two-component vapour in the collisional regime. The dispersion relation of the surface modes for the total particle density reduces in this case to that of a one-component Fermi vapour, whereas the frequencies of all other modes are shifted by the interactions.

PACS. 67.40.Db Quantum statistical theory; ground state, elementary excitations

1 Introduction

The experimental realization of Bose-Einstein condensation in confined vapours of alkali atoms [1, 2, 3, 4] has given impulse to the study of dilute quantal fluids, including vapours of fermionic atoms. Magneto-optical confinement of fermionic species has been reported for ⁶Li [5] and ⁴⁰K [6]. DeMarco et al. [7] have realized magnetic trapping of ⁴⁰K atoms in two different hyperfine states corresponding to $|F = 9/2, F_z = 9/2\rangle$ and $|F = 9/2, F_z = 7/2\rangle$, with the possibility of varying the relative ‘concentration’ of these two components of the vapour up to selective

*e-mail: tosim@bib.sns.it

removal of one of them. Earlier experimental work on double Bose condensates [8, 9] and some of the related theoretical work on the equilibrium state and on the excitation properties of bosonic mixtures [10, 11, 12, 13, 14, 15] may also be recalled at this point.

The s-wave collisions between pairs of fermions in the same hyperfine state are suppressed by the Pauli principle, so that to leading order only p-wave scattering and dipole-dipole magnetic interactions remain in a one-component, spin-polarized Fermi vapour. These effects are very weak at very low temperatures and the vapour may be treated as an ideal Fermi gas [16, 17, 18, 19]. In the two-component vapours studied by DeMarco et al. [7], however, s-wave scattering is operative between pairs of ^{40}K atoms in different hyperfine states. They have thus been able to measure the s-wave scattering length of ^{40}K , to observe directly the p-wave energy threshold law and to evaporatively cool the vapour down to 5 mK. While the s-wave scattering determined in this way for ^{40}K is repulsive (i.e. is described by a positive scattering length), a negative scattering length for ^6Li atoms holds promise of achieving a superfluid state in a mixture of ^6Li atoms prepared in two hyperfine states [20]. The insurgence of superfluidity may be revealed through the study of the elementary excitations of the vapour [21, 22, 23].

In the present work we extend to two-component interacting Fermi vapours in the normal (non-superfluid) state our former study of the small-amplitude excitations of density fluctuations in an ideal Fermi gas confined in a harmonic trap at zero temperature [24]. We make use of an equations-of-motion approach which is formulated in full generality in Sect. 2 in order to stress the analogies between the problem of present interest and that of spin dynamics and spin diffusion in a homogeneous Fermi liquid in a given state of partial spin polarization [25, 26]. The nature of the assumptions which are adopted in our further calculations on confined Fermi vapours is made more explicit and justified by this discussion.

In Sect. 3 we assume complete equilibrium for the two-component vapour under spherical harmonic confinement and evaluate the Thomas-Fermi ground-state densities upon relating the components of the kinetic stress tensor to the local densities by the ideal-gas formula. We give specific attention to three different cases, i.e. (i) the ^{40}K system studied by DeMarco et al. [7], (ii) a strong-coupling regime in which the repulsive interactions between the two components of a symmetric vapour drive their spatial separation, and (iii) a simplified description of the weak-coupling regime in a symmetric vapour. By a symmetric vapour as treated in (ii) and (iii) we mean equal numbers of particles in the two components as well as equal masses and equal confinements, as is relevant in relation to the experiments of DeMarco et al. [7]. The form obtained in (iii) for the density profile is used in Sect. 4 to obtain an analytic determination of the eigenvectors and of the dispersion relation for both in-phase and out-of-phase oscillations in a symmetric vapour in the collisional regime. The role of the interactions in comparison with the vibrational properties of an ideal one-component Fermi gas is of main interest here. Finally, Sect. 5 gives a brief summary of our main results and offers some concluding remarks.

2 Generalized quantum hydrodynamics in a two component Fermi fluid

We review in this section some general properties of the dynamics of a two-component fluid with given equilibrium densities $n_\sigma(\mathbf{r})$, σ being a component index that we shall write as $\sigma = (\uparrow, \downarrow)$ to stress the analogy with the problem of spin dynamics in a partially spin-polarized electron gas [26]. The Hamiltonian describing the fluid in the presence of external scalar potentials $V_\sigma(\mathbf{r}, t)$ is

$$\begin{aligned}
H &= \sum_{\sigma} \int d^3r \hat{\psi}_{\sigma}^{\dagger}(\mathbf{r}, t) \left[-\frac{\hbar^2}{2m_{\sigma}} \nabla_{\mathbf{r}}^2 + V_{\sigma}(\mathbf{r}, t) \right] \hat{\psi}_{\sigma}(\mathbf{r}, t) \\
&+ \frac{1}{2} \sum_{\sigma, \sigma'} \int d^3r \int d^3r' \phi_{\sigma, \sigma'}(\mathbf{r}, \mathbf{r}') \hat{\psi}_{\sigma}^{\dagger}(\mathbf{r}, t) \hat{\psi}_{\sigma'}^{\dagger}(\mathbf{r}', t) \hat{\psi}_{\sigma'}(\mathbf{r}', t) \hat{\psi}_{\sigma}(\mathbf{r}, t), \quad (2.1)
\end{aligned}$$

where $\hat{\psi}_\sigma(\mathbf{r}, t)$ are the field operators and $\phi_{\sigma,\sigma'}(\mathbf{r}, \mathbf{r}')$ the interatomic potentials. Redistributions of population in the two states are not allowed.

The equations of motions for the partial particle densities $n_\sigma(\mathbf{r}, t)$ are obtained by a standard procedure (see e.g. [27]), involving (i) the derivation of the equation of motion for the density matrix $\rho_\sigma(\mathbf{x}, \mathbf{x}'; t) = \langle \hat{\psi}_\sigma^\dagger(\mathbf{r}, t) \hat{\psi}_\sigma(\mathbf{r}, t) \rangle$ from the Hamiltonian (2.1), and (ii) projection on the diagonal $\mathbf{r} = (\mathbf{x} + \mathbf{x}')/2$. Setting $\mathbf{r}' = \mathbf{x} - \mathbf{x}'$, the result is

$$m_\sigma \frac{\partial^2 n_\sigma(\mathbf{r}, t)}{\partial t^2} = \nabla_\alpha^{(\mathbf{r})} \nabla_\beta^{(\mathbf{r})} \Pi_{\alpha\beta}^\sigma(\mathbf{r}, t) + \nabla_\alpha^{(\mathbf{r})} [n_\sigma(\mathbf{r}, t) \nabla_\alpha^{(\mathbf{r})} V_\sigma^H(\mathbf{r}, t)] + \sum_{\sigma'} \int d^3 r' \nabla_\alpha^{(\mathbf{r})} \{ [\nabla_\alpha^{(\mathbf{r})} \phi_{\sigma,\sigma'}(\mathbf{r}, \mathbf{r}')] \langle \rho_\sigma(\mathbf{r}, t) \rho_{\sigma'}(\mathbf{r}', t) \rangle_c \}, \quad (2.2)$$

where the convention of summation over repeated Cartesian indices in the derivatives has been adopted. In Eq. (2.2) we have defined the kinetic stress tensors

$$\Pi_{\alpha\beta}^\sigma(\mathbf{r}, t) = -\frac{\hbar^2}{m_\sigma} \nabla_\alpha^{(\mathbf{r}')} \nabla_\beta^{(\mathbf{r}')} \rho_\sigma(\mathbf{r} - \mathbf{r}'/2, \mathbf{r} + \mathbf{r}'/2; t) \Big|_{\mathbf{r}'=0} \quad (2.3)$$

and the mean-field potentials

$$V_\sigma^H(\mathbf{r}, t) = V_\sigma(\mathbf{r}, t) + \sum_{\sigma'} \int d^3 r' \phi_{\sigma,\sigma'}(\mathbf{r}, \mathbf{r}') n_{\sigma'}(\mathbf{r}', t). \quad (2.4)$$

The non-mean-field effects are collected in the last term on the RHS of Eq. (2.2), where $\rho_\sigma(\mathbf{r}, t)$ is the density operator and $\langle \rho_\sigma(\mathbf{r}, t) \rho_{\sigma'}(\mathbf{r}', t) \rangle_c$ is the cluster part of the density-density correlations. No assumption has as yet been made on the temperature of the fluid.

The equilibrium equations determining the density profiles $n_\sigma(\mathbf{r})$ are obtained from Eq. (2.2) by taking the static limit. The equations of motion for the density fluctuations $\delta n_\sigma(\mathbf{r}, t)$ driven by weak external potentials are then obtained by writing $n_\sigma(\mathbf{r}, t) = n_\sigma(\mathbf{r}) + \delta n_\sigma(\mathbf{r}, t)$ in Eq. (2.2) and by linearizing it. We shall go through these steps in Section 3 and 4 for a dilute two-component Fermi vapour. Here we proceed to introduce the approximations that we shall make in the dynamical treatment of Sect. 4 by discussing the non-mean-field term in Eq. (2.2).

2.1 Interdiffusion in the two component fluid

We evaluate in this section the role of collisions between fluctuations in determining damping of collective motions in the two-component fluid. As a preliminary we recall that the linearized equations of motion for the partial density fluctuations in the two-component fluid are conveniently transformed into those for the total particle density fluctuation $\delta n(\mathbf{r}, t)$ and for the concentration fluctuation $\delta M(\mathbf{r}, t)$ (the "magnetization" fluctuation in the electron gas analogue) by taking simple linear combinations of the two $\delta n_\sigma(\mathbf{r}, t)$'s (see e.g.[28]).

We consider first the dynamics of small fluctuations around a homogeneous equilibrium state, where we can appeal to the treatment given by Caccamo et al. [26] for the evaluation of the interdiffusion (or "spin diffusion") coefficient. Momentum conservation ensures that the only non-vanishing inverse relaxation time in the hydrodynamic limit is the interdiffusion one, say τ_{MM}^{-1} , which is written as

$$\tau_{MM}^{-1} = n\gamma_M / (mn_\uparrow n_\downarrow) \quad (2.5)$$

where n_\uparrow and n_\downarrow are the partial equilibrium densities, $n = n_\uparrow + n_\downarrow$ is the total density and we have assumed $m = m_\uparrow = m_\downarrow$. An exact expression for the quantity γ_M in Eq. (2.5) is obtained from the non-mean-field term in Eq. (2.2) in the appropriate hydrodynamic limit. In the case of a central pair potential this reads

$$\gamma_M = \int d^3 r (\hat{k} \cdot \nabla) \phi_{\uparrow\downarrow}(r) \frac{\partial \langle \rho_\uparrow(\mathbf{R}) \rho_\downarrow(\mathbf{R} + \mathbf{r}) \rangle_c}{\partial v_\uparrow} \quad (2.6)$$

in a reference frame where the component \uparrow is at rest and the other component is flowing with a uniform drift velocity v_\downarrow .

The Fourier transform of the non-equilibrium correlation function in Eq. (2.6) is evaluated in a binary collision approximation by the decoupling procedure used by Baym [29] in treating the electrical resistance of metals (see also Kadanoff and Baym [30]). Namely,

$$\text{ImF.T.} \{ \langle \rho_{\uparrow}(\mathbf{R}) \rho_{\downarrow}(\mathbf{R} + \mathbf{r}) \rangle_c \}_{\mathbf{k}} = \frac{1}{2} n \hbar \phi_{\uparrow\downarrow}(k) \int_{-\infty}^{\infty} \frac{d\omega}{2\pi} [\tilde{S}_{\uparrow\uparrow}(\mathbf{k}, \omega) \tilde{S}_{\downarrow\downarrow}(-\mathbf{k}, -\omega) - \tilde{S}_{\uparrow\uparrow}(-\mathbf{k}, -\omega) \tilde{S}_{\downarrow\downarrow}(\mathbf{k}, \omega)] , \quad (2.7)$$

where $\tilde{S}_{\sigma\sigma}(\mathbf{k}\omega)$ is the van Hove dynamic structure factor of each component in the non-equilibrium state. For the dilute Fermi fluid of present interest we can replace the interaction potential in Eq. (2.7) by a contact interaction and $\tilde{S}_{\sigma\sigma}(\mathbf{k}\omega)$ by the ideal-gas value corresponding to a displaced Fermi sphere for the \downarrow component. Following the lines of the calculation given in Ref. [26] and taking for simplicity $n_{\uparrow} = n_{\downarrow}$ in Eq. (2.5), we find to leading order in the temperature T the result

$$\tau_{MM}^{-1} = (4\pi m a_{\uparrow\downarrow}^2 E_F^2 / 3\hbar^3) (T/T_F)^2 . \quad (2.8)$$

Here, $a_{\uparrow\downarrow}$ is the (triplet) scattering length, E_F is the Fermi energy and $T_F = E_F/k_B$. This result could also be obtained directly from Eq. (6.8) in Ref. [26] upon replacing a screened Coulomb interaction by a contact interaction.

The result given in Eq. (2.8) above for a homogeneous, two-component Fermi fluid can now be used for an estimate of the role of collisions in a confined Fermi fluid. We replace the Fermi energy E_F by its local value, which in the case of harmonic confinement in a spherical trap characterized by a frequency ω_f is

$$E_F = (3N)^{1/3} \hbar \omega_f \quad (2.9)$$

with N the total number of fermions. Hence,

$$(\omega_f \tau_{MM})^{-1} = (4\pi/3^{1/3}) (N^{1/3} a_{\uparrow\downarrow} / a_{ho})^2 (T/T_F)^2 \quad (2.10)$$

$a_{ho} = (\hbar/m\omega_f)^{1/2}$ being the harmonic-oscillator length. A similar result has been reported recently by Vichi and Stringari [31] from a collision-integral approach.

In summary, because of momentum conservation the damping processes in the hydrodynamic limit of a two-component Fermi fluid are associated with collisions between the two components and affect only their relative motions. These processes vanish quadratically with decreasing temperature because of Fermi statistics (see also [25]). A collisional regime may nevertheless be established by scattering against impurities (see for instance the work of Ruckenstein and Lévy [32] on spin dynamics in paramagnetic quantum fluids). We turn below to an estimate of these collision processes in the normal Fermi fluid of present interest.

2.2 Collisional regime via impurity scattering

A collisional regime is established in the low-temperature vapour *for both in-phase and out-of-phase modes of motion of the two components* when the inequality

$$\omega\tau \ll 1 \quad (2.11)$$

holds, τ being the collision time for scattering of fermions against impurities and ω being on the scale of the trap frequency ($\omega \simeq \omega_f$) for low-frequency modes.

For an estimate of the needed number N_s of scatterers we take the impurities as cold atoms with a mean velocity which is negligible relative to that of the fermions. We can then write $\tau = l/v$, l and v being the mean free path and the average speed of a fermion. We have $l = \Sigma^{-1}$, where Σ is the macroscopic cross-section given by $\Sigma = n_s \sigma$ in terms of the density n_s of scatterers and of the cross-section σ for fermion-impurity scattering (see for instance Ref. [33]).

Setting $n_s = N_s(4\pi a_{ho}^3/3)^{-1}$ and $\sigma = 4\pi a_{sc}^2$ with a_{sc} the fermion-impurity scattering length, and taking $v = (3E_F/4m)^{1/2}$ with E_F given by Eq. (2.9), we find

$$\omega_f \tau = \frac{(4/27)^{1/2}}{N_s(3N)^{1/6}} \left(\frac{a_{ho}}{a_s} \right)^2 \quad (2.12)$$

For illustrative purposes we consider the case of ^{39}K or ^{41}K bosonic impurities in the gas of ^{40}K fermions studied by DeMarco et al. [7] ($N \simeq 10^7$ and $\omega_f \simeq 209 \text{ s}^{-1}$, the latter being the geometric mean of the radial and axial frequencies in the experiment). From the known values of the ^{39}K - ^{40}K and ^{41}K - ^{40}K scattering lengths ($a_s \simeq 3600$ and $a_s \simeq 93$ Bohr radii, respectively) we find that a number of ^{39}K impurities of order $N_s \simeq 10^{-6}N$, or of ^{41}K impurities of order $N_s \simeq 10^{-3}N$, would suffice to verify the inequality (2.11) with $\omega = \omega_f$.

We conclude, therefore, that a collisional regime can easily be established for the low-frequency excitations of trapped Fermi vapours. This regime reflects rather directly the quantal statistics of the vapour [24] and we study it for the two-component Fermi fluid in Sect. 4 below. Excitations in the collisionless regime are of less interest, since they mostly reflect the frequency of the trap [24, 31].

3 Equilibrium density profiles in spherical confinement

As already discussed in Sect. 1, we treat a dilute two-component Fermi gas at zero temperature in which only s -wave scattering between pairs of fermions in different hyperfine states is operative. This coupling is described by the parameter $f = 4\pi\hbar^2 a_{\uparrow\downarrow}/m$. In the experimentally relevant situation the two populations have not only the same mass but also essentially identical numbers and trap frequencies. However, we shall impose the equality $N_{\uparrow} = N_{\downarrow} = N/2$ only later below.

We take the gas as being statically in the equilibrium state and dynamically in the collisional regime. As in our earlier work [24], we relate the kinetic stress tensor of each component to its local density by the homogeneous Fermi gas formula,

$$\Pi_{\alpha\beta}^{\sigma}(\mathbf{r}, t) = \delta_{\alpha\beta} \frac{2}{5} A [n_{\sigma}(\mathbf{r}, t)]^{5/3} \quad (3.1)$$

where $A = \hbar^2(6\pi^2)^{2/3}/2m$. Such a local density approximation assumes that the length scale for the variation of the density profiles in space is large relative to the inverse Fermi wave number k_f^{-1} and to the length c/ω , with ω the excitation frequency and c the velocity of sound propagation in the homogeneous fluid.

The equilibrium density profiles are then easily obtained from the static limit of Eq. (2.2) in the mean-field approximation. They have the Thomas-Fermi form,

$$n_{\sigma}(\mathbf{r}) = \theta[\epsilon_{\sigma} - V_{\sigma}(\mathbf{r}) - f n_{\bar{\sigma}}(\mathbf{r})] \left\{ A^{-1} [\epsilon_{\sigma} - V_{\sigma}(\mathbf{r}) - f n_{\bar{\sigma}}(\mathbf{r})] \right\}^{3/2}, \quad (3.2)$$

where $\bar{\sigma}$ denotes the component different from σ . In Eq. (3.2) $V_{\sigma}(\mathbf{r})$ are the static confining potentials and ϵ_{σ} are the chemical potentials, to be determined from the condition $N_{\sigma} = \int d^3r n_{\sigma}(\mathbf{r})$. We emphasize that the N_{σ} 's are fixed, *i.e.* these equations do not allow for redistributions of population in the two hyperfine states.

In the same approximation the total energy of the vapour is the sum of three terms, *i.e.* a kinetic energy E_{kin} , a potential energy E_{ho} and an interaction energy E_{int} . These are

$$E_{kin} = (6\pi^2)^{2/3} \frac{3\hbar^2}{5m} \sum_{\sigma} \int d^3r [n_{\sigma}(\mathbf{r})]^{5/3}, \quad (3.3)$$

$$E_{ho} = \sum_{\sigma} \int d^3r n_{\sigma}(\mathbf{r}) V_{\sigma}(\mathbf{r}) \quad (3.4)$$

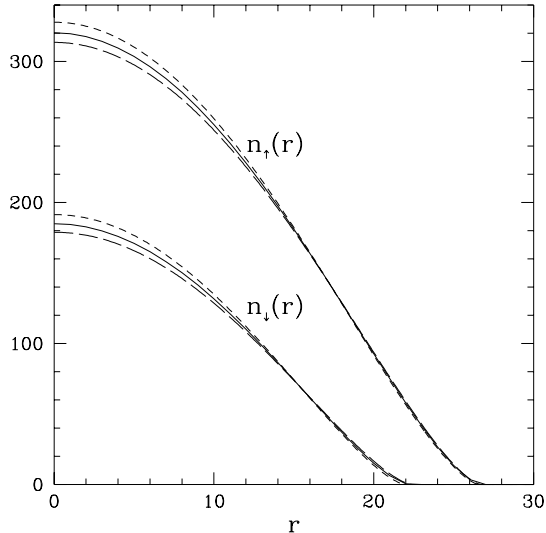


FIGURE 1: Density profiles $n_{\uparrow}(r)$ and $n_{\downarrow}(r)$ (in units of a_{ho}^{-3}) versus distance r from the centre of a spherical trap (in units of a_{ho}) in a mixture of 10^7 fermions at composition $N_{\uparrow}/N_{\downarrow} = 3$. The long (short) dashed curves show the profiles corresponding to an s -wave scattering length $a_{\uparrow\downarrow} = 157 a_B$ ($a_{\uparrow\downarrow} = -157 a_B$), relatively to the case of the ideal mixture (full curves).

and

$$E_{int} = \sum_{\sigma} \int d^3r n_{\uparrow}(\mathbf{r}) n_{\downarrow}(\mathbf{r}) \quad (3.5)$$

These will be helpful in understanding the behaviour of the vapour at strong coupling in Sect. 3.2.

3.1 An illustrative example for a weakly coupled ^{40}K vapour

Figure 1 reports the numerical results that we obtain from Eq. (3.2) for the density profiles in a gas subject to spherical harmonic confinement, with system parameters chosen after the experiment of DeMarco *et al.* [7] ($\omega_f = (\omega_{\parallel}\omega_{\perp}^2)^{1/3} = 209 \text{ s}^{-1}$, $N = 10^7$ and $a_{\uparrow\downarrow} = 157$ Bohr radii) but at composition $N_{\uparrow}/N_{\downarrow} = 3$. The cases $a_{\uparrow\downarrow} = -157 a_B$ and $a_{\uparrow\downarrow} = 0$ are also shown.

Evidently, the effects of the interactions are small in this situation and very simple to understand: a repulsion (attraction) between the two components disfavours (favours) their overlap in the central part of the trap.

3.2 Spatial separation of the two components at strong coupling

We may expect that in the case of repulsive interactions, with increasing coupling strength and still barring transitions between the two hyperfine levels as already noted under Eq. (3.2), the gas will be led to diminish its total energy by reducing the spatial overlap between the two components. Figure 2 shows how such symmetry breaking occurs in a spherical trap, for $N_{\uparrow} = N_{\downarrow}$ and under the condition that overall spherical symmetry be maintained. In this case one component is pushed away from the centre of the trap and the gas configuration becomes that of a central core enriched in one component and surrounded by a spherical shell enriched in the other.

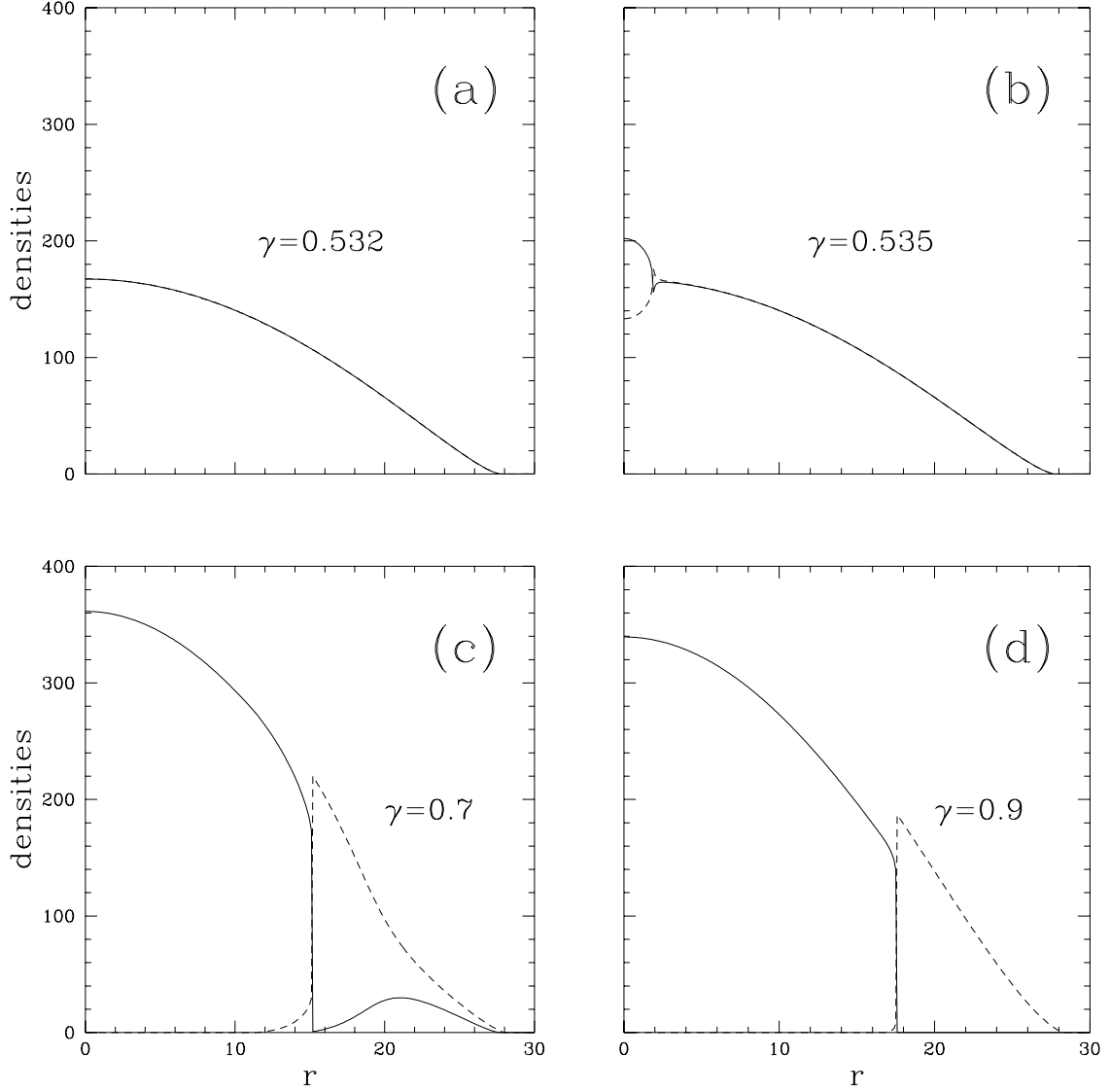


FIGURE 2: Density profiles (in units of a_{ho}^{-3}) versus distance r from the centre of a spherical trap (in units of a_{ho}) in a symmetric mixture of fermions, at various values of the coupling strength parameter γ . In (a), the profiles of the two components are still in complete overlap. Spatial symmetry breaking is first visible in (b). Separation of the two components (shown by full and dashed curves) continues through (c) and (d).

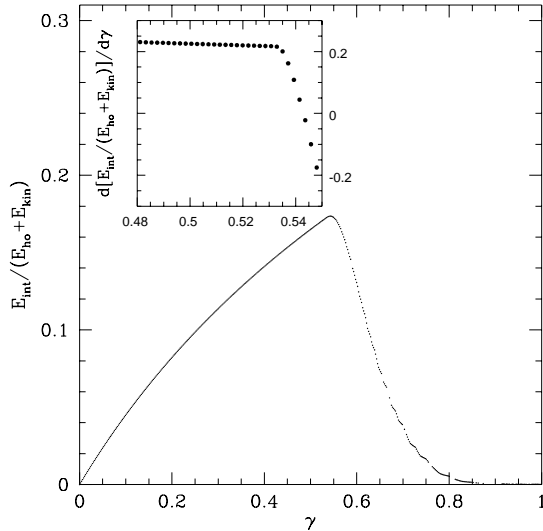


FIGURE 3: The ratio of the interaction energy E_{int} to the sum $E_{ho} + E_{kin}$ of the harmonic-oscillator and kinetic energies, plotted against the coupling strength $\gamma \simeq 0.5N^{1/6}(a_{\uparrow\downarrow}/a_{ho})$ for a symmetric mixture of fermions in spherical confinement. The inset shows the first derivative of the same function.

The symmetry breaking is driven by the competition between the repulsive interaction energy, favouring spatial separation of the components, and the kinetic energy disfavours localization. Evidently and in contrast to the behaviour illustrated in Figure 2, a gas confined in an axially symmetric trap will tend to reduce its energy *via* relative shifts in the centres of the two clouds. A rich phase diagram will ensue if "spin flips" between the two hyperfine states are also allowed. In the following we estimate the critical coupling strength at which spatial symmetry breaking occurs in terms of the number of fermions (or alternatively of the $a_{\uparrow\downarrow}$ scattering length) for the case illustrated in Figure 2.

The four cases of density profiles illustrated in Figure 2 are labelled by a parameter γ , which is defined by

$$\gamma = \alpha N^{1/6} (a_{\uparrow\downarrow}/a_{ho}) \quad (3.6)$$

with $\alpha = 2^{1/3}3^{1/6}(8192/2835\pi^2)$ [31]. In fact the value of γ in Eq. (3.6) is obtained as $\gamma = [E_{int}/(E_{ho} + E_{kin})]_0$ when the ratio $E_{int}/(E_{ho} + E_{kin})$ is calculated from the density profile of the Fermi gas in the absence of interactions. Figure 3 reports the true values of $E_{int}/(E_{ho} + E_{kin})$ against γ for the system described in Figure 2. The (obvious) linear shape of this function at weak couplings gently bends over with increasing coupling, until an almost sharp break occurs at spatial symmetry breaking. This is emphasized in the inset in Figure 3 giving the derivative of $E_{int}/(E_{ho} + E_{kin})$ with respect to γ . We have checked that the same plot is obtained for $E_{int}/(E_{ho} + E_{kin})$ by varying $a_{\uparrow\downarrow}/a_{ho}$ at constant N and by varying N at constant $a_{\uparrow\downarrow}/a_{ho}$.

In the experiments of DeMarco et al. [7] on ^{40}K with $N \simeq 10^7$, the value of γ is $\gamma \simeq 0.022$ i.e. still very far from the critical value $\gamma_c \simeq 0.535$ for the symmetry breaking illustrated in Figures 2 and 3. The weak dependence of γ on N in Eq. (3.6) implies that a number of ^{40}K atoms of order 10^{15} would have to be reached if all other system parameters remain the same. A parallel increase in the ratio $a_{\uparrow\downarrow}/a_{ho}$ as suggested by Eq. (3.6) would evidently be helpful in relaxing such stringent condition.

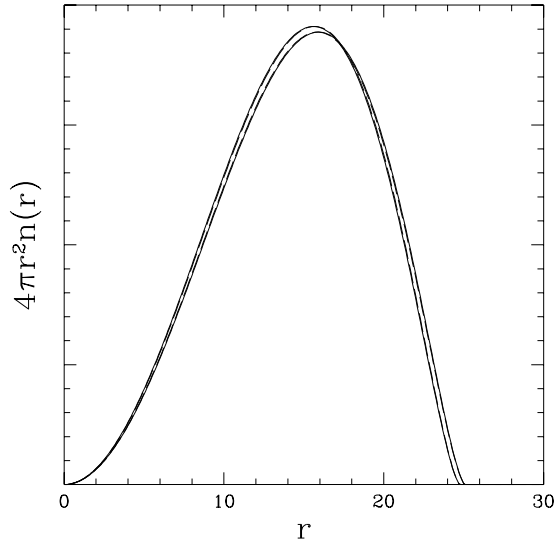


FIGURE 4: Illustrating the accuracy of the approximate form (3.8) of the particle distribution $4\pi r^2 n(r)$ (dashed curves) relative to the full Thomas-Fermi profile (full curves), for a symmetric mixture of fermions in the two cases $\gamma = \pm 0.022$.

3.3 Approximate form of the density profile for a symmetric vapour at weak coupling

In the case $N_\uparrow = N_\downarrow$ the shape of the total density profile $n(\mathbf{r}) = n_\uparrow(\mathbf{r}) + n_\downarrow(\mathbf{r})$ at weak coupling is well represented by a form which is suitable for the analytic study of the eigenmodes of the gas that we report in Sect. 4 below. From Eq. (3.2) the Thomas-Fermi density profile is

$$n(\mathbf{r}) = 2A^{-3/2} \left[\epsilon_F - \frac{1}{2} m \omega_f^2 r^2 - \frac{f}{2} n(\mathbf{r}) \right]^{3/2}, \quad (3.7)$$

for $r \leq R_F$, where $R_F = (2\epsilon_F/m\omega_f^2)^{1/2}$ and $\epsilon_F = \epsilon_\uparrow = \epsilon_\downarrow$ is the chemical potential of the mixture. At weak coupling the profile (3.7) can be approximated by

$$n(\mathbf{r}) = \frac{8N}{\pi^2 R_F^3} (1 - r^2/R_F^2)^{3/2} \theta(1 - r^2/R_F^2), \quad (3.8)$$

where ϵ_F and R_F still are the true chemical potential and the Fermi radius in the interacting mixture. The form (3.8) is adjusted to preserve normalization to N as well as the value of R_F .

Figure 4 compares the approximate form (3.8) with the correct Thomas-Fermi form (3.7) at $\gamma = \pm 0.022$ by plotting the function $4\pi r^2 n(r)$. The phase-space factor $4\pi r^2$ masks the small differences that would be present in the two forms of $n(\mathbf{r})$ near the centre of the trap. On the other hand, preserving the correct value of the Fermi radius in the approximate form (3.8) is crucial in view of the boundary conditions to be imposed in the determination of the eigenmodes of the vapour.

As a final remark we notice that the profile in Eq. (3.8) has the same form as for an ideal one-component Fermi gas [34]. This fact is crucial for the analytic treatment of the dynamics of density fluctuations in a weakly coupled symmetric mixture, that we give in the next section.

4 Dynamics of density fluctuations

The equations of motions (2.2), after linearization in the partial density fluctuations and adopting (i) the mean-field approximation ($\langle \rho_\sigma(\mathbf{r}, t) \rho_{\sigma'}(\mathbf{r}', t) \rangle_c = 0$) and (ii) the local density approximation for the kinetic stress tensor (Eq. (3.1)), reduce to

$$m \frac{\partial^2 n_\sigma(\mathbf{r})}{\partial t^2} = \nabla^2 \left[\frac{2}{3} A n_\sigma^{2/3}(\mathbf{r}) \delta n_\sigma(\mathbf{r}, t) \right] + \nabla \cdot \{ \delta n_\sigma(\mathbf{r}, t) \nabla [V_\sigma(\mathbf{r}) + f n_{\bar{\sigma}}(\mathbf{r}, t)] + f n_\sigma(\mathbf{r}) \nabla \delta n_{\bar{\sigma}}(\mathbf{r}, t) \} \quad (4.1)$$

at resonance (*i.e.* for $V_\sigma(\mathbf{r}, t) = V_\sigma(\mathbf{r})$). With the help of the equilibrium conditions (3.2), and taking Fourier transforms with respect to the time variable, Eq. (4.1) can be written as

$$-m\omega^2 \delta n_\sigma(\mathbf{r}, \omega) = \frac{1}{3} A \left[2n_\sigma^{2/3}(\mathbf{r}) \nabla^2 + \nabla(n_\sigma^{2/3}) \cdot \nabla - \nabla^2(n_\sigma^{2/3}) \right] \delta n_\sigma(\mathbf{r}, \omega) + \left\{ [\epsilon_{\bar{\sigma}} - V_{\bar{\sigma}}(\mathbf{r}) - A n_{\bar{\sigma}}^{2/3}] \nabla^2 - \nabla[V_{\bar{\sigma}}(\mathbf{r}) + A n_{\bar{\sigma}}^{2/3}] \cdot \nabla \right\} \delta n_{\bar{\sigma}}(\mathbf{r}, \omega) \quad (4.2)$$

Evidently, Eq. (4.2) describes a two-by-two eigenvalue problem for the coupled partial density fluctuations, which is to be solved numerically in the general case.

The problem is considerably simplified in the case of a symmetric mixture ($m_\uparrow = m_\downarrow$, $N_\uparrow = N_\downarrow$ and $V_\uparrow(\mathbf{r}) = V_\downarrow(\mathbf{r})$), these conditions being well satisfied in the experiments of DeMarco et al. [7]. In this case the dynamical equations (4.2) lead to separate equations of motion for the total density fluctuations $\delta n(\mathbf{r}, \omega) = \delta n_\uparrow(\mathbf{r}, \omega) + \delta n_\downarrow(\mathbf{r}, \omega)$ and for the concentration fluctuations $\delta M(\mathbf{r}, \omega) = \delta n_\uparrow(\mathbf{r}, \omega) - \delta n_\downarrow(\mathbf{r}, \omega)$. The eigenvalue equation for $\delta n(\mathbf{r}, \omega)$ reads

$$-m\omega^2 \delta n(\mathbf{r}, \omega) = \nabla \cdot \left(\frac{2}{3} A (n/2)^{2/3} \nabla \delta n(\mathbf{r}, \omega) - \frac{A}{3} (\nabla(n/2)^{2/3}) \delta n \right) + (\epsilon_F - V(\mathbf{r}) - A(n/2)^{2/3}) \nabla \delta n(\mathbf{r}, \omega) . \quad (4.3)$$

Similarly, the eigenvalue equation for $\delta M(\mathbf{r}, \omega)$ is

$$-m\omega^2 \delta M(\mathbf{r}, \omega) = \nabla \cdot \left(\frac{2}{3} A (n/2)^{2/3} \nabla \delta M - \frac{A}{3} (\nabla(n/2)^{2/3}) \delta M(\mathbf{r}, \omega) \right) - (\epsilon_F - V(\mathbf{r}) - A(n/2)^{2/3}) \nabla \delta M(\mathbf{r}, \omega) . \quad (4.4)$$

Equations (4.3) and (4.4) can be solved analytically by the technique used in our earlier work on the ideal one-component Fermi gas [24], if the form (3.8) is adopted for the equilibrium profile. As already discussed in Sect. 3.3, Eq. (3.8) becomes accurate at small coupling. We shall again impose that the solutions vanish continuously at the cloud boundary, as a consequence of Fermi statistics giving a high cost in kinetic energy to rapid variations of the densities in space. For both in-phase and out-of-phase motions of the two components, the frequency eigenvalues depend on a parameter C given by

$$C = (3N)^{2/3} (\hbar\omega_f / \epsilon_F)^2 \quad (4.5)$$

This quantity is the square of the ratio of the ideal Fermi energy to the true Fermi energy and hence, in the case of repulsive interactions where ϵ_F increases with the scattering length, is limited from above by the inequality $C < 1$. All the mathematical details of the solution of Eqs. (4.3) and (4.4) are given in Appendix A. Here we report only the main results.

4.1 Small oscillations of total density fluctuations

The eigenfunctions of the total density oscillations vanish at the Fermi radius $r = R_F$ provided $C < 3$, in a way which depends on the parameter C and hence on the strength of the interactions (see Appendix A.1 for their detailed expressions).

The corresponding eigenfrequencies are labelled by the angular momentum number l and by an integer n representing the number of internal nodes in the density fluctuation profile. The dispersion relation is

$$(\omega_{nl}/\omega_f)^2 = l + 2n + \frac{n}{3}(3 - C)(2n + 2l + 1) \quad (4.6)$$

The ideal Fermi gas limit corresponds to $C = 1$ and in this case Eq. (4.6) yields back our earlier result [24]. More generally, the dispersion relation (4.6) reduces to that of the ideal Fermi gas only for the surface modes (i.e. for $n = 0$). Instead, the frequencies of the modes with $n > 0$ are shifted by the interactions.

The above results are easily extended to evaluate the low-frequency modes in an axially symmetric confinement (see e.g. [24]). As discussed in Sect. 2, damping of these modes will set in when $\omega\tau \simeq 1$ for scattering against cold-atom impurities.

4.2 Small oscillations of concentration fluctuations

The eigenfunctions vanish at the Fermi radius only if $C > 3/5$ (see Appendix A.2 for the details). This inequality marks the breakdown of the present approximation in the case of repulsive interactions. Under this restriction the dispersion relation for concentration fluctuations having n internal nodes is

$$(\omega_{nl}/\omega_f)^2 = (l + 2n)(2C - 1) + \frac{n}{3}(5C - 3)(2n + 2l + 1) \quad (4.7)$$

Of course, for both surface ($n = 0$) and bulk ($n \neq 0$) modes these frequencies differ from those of density fluctuations in the ideal one-component Fermi gas.

Damping of these modes will arise not only from scattering against cold-atom impurities but also from thermal excitations (see Sect. 2.1). A detailed discussion of the latter damping for the spin dipole excitation has been given by Vichi and Stringari [31].

5 Summary and concluding remarks

In summary, the focus of this work has been on two-component mixtures of fermionic atoms in dilute-vapour states and subject to spherical harmonic confinement at zero temperature. The main motivation has come from the experiments of DeMarco et al. [6] on vapours of ^{40}K atoms magnetically trapped in two different hyperfine states.

The generalized hydrodynamic equations of the mixture have allowed us to discuss the damping mechanisms from correlations between partial density fluctuations beyond mean field terms. Because of momentum conservation in a pure two-component Fermi fluid the dissipation processes in the hydrodynamic limit are associated with collisions between the two components and these vanish quadratically with temperature because of Fermi statistics. We have then discussed how a collisional regime may nevertheless arise for both global and relative density fluctuations at very low temperature from collisions of the Fermi fluid against cold impurity atoms. We have seen that the establishment of a collisional regime, in which the dynamical behaviour of the fluid reflects the quantal statistics, is not subject to especially severe restrictions on the strength of the fermion-impurity scattering nor on the number of impurities.

We have then evaluated ground-state properties and small-amplitude excitations of such a two-component Fermi fluid in a collisional regime. We have shown that, whereas the role of the interactions in determining the equilibrium density profiles is still very weak in the cases experimentally studied so far, a rich phase diagram will emerge as the coupling strength is increased and/or redistribution of the components between magnetic states becomes allowed. The relevant coupling strength depends in a simple manner on the number of fermions in the trap and on the ratio of the scattering length to the harmonic-oscillator length. Finally, we have shown how the problem of small-amplitude oscillations of both the total particle density and the concentration density in a weakly coupled symmetric mixture is amenable to full analytic solution in parallel with the analogous problem for an ideal Fermi gas.

This work is supported by the Istituto Nazionale di Fisica della Materia through the Advanced Research Project on BEC. One of us (MA) wishes to thank the Abdus Salam International Centre for Theoretical Physics for their hospitality during the final stages of this work.

A Solution of equations (4.3) and (4.4)

We give in this Appendix the details of the analytic solution of the eigenvalue equations (4.3) and (4.4) and the expressions for their eigenfunctions.

A.1 Total density fluctuations

From Eqs. (4.3) and (3.8) we find

$$[6(\omega/\omega_f)^2 + C\nabla_x^2(x^2)]\delta n(\mathbf{x}, \omega) + (3 - C)(1 - x^2)\nabla_x^2\delta n(\mathbf{x}, \omega) - (3 - 2C)\nabla(x^2) \cdot \nabla\delta n(\mathbf{x}, \omega) = 0 \quad (\text{A.1})$$

where $x = r/R_F$. The solutions of Eq. (A.1) have the form $\delta n(\mathbf{x}, \omega) = x^l F(x^2) Y_l^m(\theta, \phi)$, because of spherical symmetry. Setting $x^2 = y$, we determine the function $F(y)$ from Eq. (A.1) by means of the Fuchs method for solving an ordinary differential equation in a series form around regular singular points [35]. This method sets

$$F(y) = (1 - y)^s \sum_{k=0}^{\infty} a_k (1 - y)^k \quad (\text{A.2})$$

and yields $s = C/(3 - C)$ together with the recurrence relation for the coefficients a_k ,

$$2(s + k + 1)(s + k - 3b + 2)\frac{a_{k+1}}{a_k} = -3b(\omega/\omega_f)^2 - 3(3b - 1) + l(2 - 3b) + (s + k)[2(s + k - 1) + 2l - 6b + 7]. \quad (\text{A.3})$$

Here, $b = (3 - C)^{-1}$. The eigenfunctions vanish at the boundary for $C < 3$.

The eigenfrequencies are obtained from Eq. (A.3) by asking that the solutions reduce to polynomials of degree $n + s$, i.e. $a_{n+1} = 0$ for an integer n representing the number of internal nodes of the density fluctuation profile. This yields the dispersion relation reported in Eq. (4.6) of the main text.

A.2 Concentration fluctuations

From Eqs. (4.4) and (3.8) we get

$$[6(\omega/\omega_f)^2 + C\nabla_x^2(x^2)]\delta M(\mathbf{x}, \omega) + (5C - 3)(1 - x^2)\nabla_x^2\delta M(\mathbf{x}, \omega) + (3 - 4C)\nabla(x^2) \cdot \nabla\delta M(\mathbf{x}, \omega) = 0 \quad (\text{A.4})$$

We look for solutions having the form $\delta M(\mathbf{x}, \omega) = x^l G(x^2) Y_l^m(\theta, \phi)$ and set $x^2 = y$ to find the differential equation obeyed by the function $G(y)$,

$$2(5C - 3)y(1 - y)\frac{d^2 G(y)}{dy^2} + [(5C - 3)(2l + 3)(1 - y) + 2y(3 - 4C)]\frac{dG(y)}{dy} + (3(\omega/\omega_f)^2 + 3C + l(3 - 4C))G(y) = 0 \quad (\text{A.5})$$

Following again the Fuchs method we set

$$G(y) = (1 - y)^s \sum_{k=0}^{\infty} a_k (1 - y)^k \quad (\text{A.6})$$

and from the indicial equation for Eq. (A.5) we find $s = C/(5C - 3)$. Therefore, the solutions will vanish at the boundary of the cloud only if $C > 3/5$.

The coefficients of the series in Eq. (A.6) obey the recurrence relation

$$2(s+k+1)[(s+k)(5C-3)-3+4C]\frac{a_{k+1}}{a_k} = -3(\omega/\omega_f)^2 - [3C+l(3-4C)] + (s+k)[(5C-3)(2s+2k+2l+1)+2(4C-3)]. \quad (\text{A.7})$$

By asking again for polynomial solutions, we obtain the dispersion relation for concentration fluctuations having n internal nodes as given in Eq. (4.7) of the main text.

References

- [1] M. H. Anderson, J. R. Ensher, M. R. Matthews, C. E. Wieman, and E. A. Cornell, *Science* **269**, 198 (1995).
- [2] K. B. Davis, M. O. Mewes, M. R. Andrews, N. J. van Druten, D. S. Durfee, D. M. Kurn, and W. Ketterle, *Phys. Rev. Lett.* **75**, 3969 (1995).
- [3] C. C. Bradley, C. A. Sackett, J. J. Tollett, and R. G. Hulet, *Phys. Rev. Lett.* **75**, 1687 (1995), see also C. C. Bradley, C. A. Sackett, and R. G. Hulet, *Phys. Rev. Lett.* **78**, 985 (1997).
- [4] C. C. Bradley, C. A. Sackett, and R. G. Hulet, *Phys. Rev. Lett.* **78**, 985 (1997).
- [5] W. McAlexander, E. Abraham, N. Ritchie, C. J. Williams, H. Stoof, and R. Hulet, *Phys. Rev. A* **51**, R871 (1995).
- [6] F. S. Cataliotti, E. A. Cornell, C. Fort, M. Inguscio, F. Marin, M. Prevedelli, L. Ricci, and G. M. Tino, *Phys. Rev. A* **57**, 1136 (1998).
- [7] B. DeMarco, J. L. Bohm, J. P. Burke, Jr., M. Holland, and D. S. Jin, *Phys. Rev. Lett.* **82**, 4208 (1999).
- [8] C. J. Myatt, E. A. Burt, R. W. Ghrist, E. A. Cornell, and C. E. Wieman, *Phys. Rev. Lett.* **78**, 586 (1997).
- [9] D. S. Hall, M. R. Matthews, J. R. Ensher, C. E. Wieman, and E. A. Cornell, *Phys. Rev. Lett.* **81**, 1539 (1998).
- [10] B. Esry, C. Greene, J. B. Jr., and J. Bohn, *Phys. Rev. Lett.* **78**, 3594 (1997).
- [11] R. Graham and D. Walls, *Phys. Rev. A* **57**, 484 (1998).
- [12] B. Esry and C. Greene, *Phys. Rev. A* **57**, 1265 (1998).
- [13] P. Öhberg and S. Stenholm, *Phys. Rev. A* **57**, 1272 (1998).
- [14] H. Pu and N. P. Bigelow, *Phys. Rev. Lett.* **80**, 1130 (1998).
- [15] H. Pu and N. Bigelow, *Phys. Rev. Lett.* **80**, 1134 (1998).
- [16] D. A. Butts and D. S. Rokhsar, *Phys. Rev. A* **55**, 4346 (1997).
- [17] J. Schneider and H. Wallis, *Phys. Rev. A* **57**, 1253 (1998).
- [18] H. T. C. Stoof and M. Houbiers, cond-mat/9808171 (unpublished).
- [19] M. Amoruso, A. Minguzzi, S. Stringari, M. P. Tosi, and L. Vichi, *Eur. Phys. J. D* **4**, 261 (1998).
- [20] M. Houbiers, R. Ferweda, H. T. C. Stoof, W. I. McAlexander, C. A. Sackett, and R. G. Hulet, *Phys. Rev. A* **56**, 4864 (1997).
- [21] W. Zhang, C. A. Sackett, and R. G. Hulet, *Phys. Rev. A* **60**, 504 (1999).
- [22] M. A. Baranov and D. S. Petrov, cond-mat/9901108 (unpublished).
- [23] G. Bruun and C. W. Clark, cond-mat/9906392 (unpublished).
- [24] M. Amoruso, I. Meccoli, A. Minguzzi, and M. Tosi, cond-mat/9907370 and *Eur. Phys. J. D*, in press (unpublished).

- [25] A. Abrikosov and I. Khalatnikov, Rep. Progr. Phys. **22**, 329 (1959).
- [26] C. Caccamo, G. Pizzimenti, and M. Tosi, N. Cimento B **31**, 329 (1976).
- [27] A. Minguzzi, M. Chiofalo, and M. Tosi, Phys. Lett. A **236**, 237 (1997).
- [28] D. Kim, H. Pradhaude, and B. Schwartz, Phys. Rev. Lett. **23**, 419 (1969).
- [29] G. Baym, Phys. Rev. **135**, 1691 (1964).
- [30] L. Kadanoff and G. Baym, *Quantum Statistical Mechanics* (Benjamin, New York, 1962).
- [31] L. Vichi and S. Stringari, cond-mat/9905154 and Phys. Rev. A, in press (unpublished).
- [32] A. Ruckenstein and L. Lévy, Phys. Rev. B **39**, 183 (1989).
- [33] A. Weinberg and E. Wigner, *The Physical Theory of Neutron Chain Reactors* (University of Chicago Press, Chicago, 1958), p.24.
- [34] K. Mølmer, Phys. Rev. Lett. **80**, 1804 (1998).
- [35] C. M. Bender and S. A. Orszag, *Advanced Mathematical Methods for Scientists and Engineers* (McGraw-Hill, New York, 1978).